

PREPRINT.

Ilker Tari, "Natural Convection Simulations and Numerical Determination of Critical Tilt Angles for a Parallel Plate Channel," Energy Conversion and Management, Vol. 51, No. 4, pp. 685-695 (2010).

# Natural convection simulations and numerical determination of critical tilt angles for a parallel plate channel

Ilker Tari

Middle East Technical University (METU)

Mechanical Engineering Dept. E-206

Ankara, 06531

Turkey

phone: +90 312 210 2551

fax: +90 312 210 2536

e-mail: itari@metu.edu.tr

## Abstract

Three dimensional laminar unsteady natural convection flow of incompressible air between two inclined parallel plates is analyzed by using spectral methods. The channel that is periodical in streamwise and spanwise directions is heated from below. The motivation behind the study is to perform simulations for a domain representing a bottom heated, open ended and inclined enclosure that appears mostly in solar energy applications. The governing equations are solved using a pseudospectral solver in order to obtain velocity and temperature fields in the channel, accurately. Fourier series and Chebyshev polynomial expansions are used for the variables. The standard Boussinesq approximation is used to include density variation. Modified Adams-Bashforth / Crank-Nicolson Semi Implicit time stepping is used for stability. By using the obtained temperature distribution between the plates, the local and the average Nusselt numbers (Nu) are calculated. The Nu values are correlated with the tilt angle for fixed Rayleigh numbers (Ra) or for a fixed Ra times cosine of the tilt angle. By observing the changes in flow structures, the critical tilt angles for air at which the maximum and the minimum heat fluxes occur are determined. There is a very good agreement with the present results and the available empirical correlations in the literature. Moreover, the present study also explores the instabilities beyond the lower and upper tilt angle limits of the experimental studies in the literature.

*Keywords:* Natural convection; parallel plate channel; inclined channel; spectral methods; solar energy; semi-implicit time stepping

## PREPRINT.

Ilker Tari, "Natural Convection Simulations and Numerical Determination of Critical Tilt Angles for a Parallel Plate Channel," Energy Conversion and Management, Vol. 51, No. 4, pp. 685-695 (2010).

### List of Symbols

ABBDI2	Adams-Bashforth / 2 <sup>nd</sup> Order Backward-Differencing
ABCN	Adams-Bashforth / Crank-Nicolson
FFT	Fast Fourier Transform
<b>g</b>	gravitational acceleration vector
<i>h</i>	convection heat transfer coefficient (W/m <sup>2</sup> K)
<i>k</i>	thermal conductivity (W/m.K)
<i>L<sub>x</sub>, L<sub>y</sub>, L<sub>z</sub></i>	dimensions of solution domain
MABCN	Modified Adams-Bashforth / Crank-Nicolson
Nu	Nusselt Number
<i>p</i>	pressure (Pa)
PV	photovoltaic
Pr	Prandtl Number
R <sup>2</sup>	Coefficient of determination
Ra	Rayleigh Number
Re	Reynolds Number
<i>t</i>	time (s)
<i>T</i>	temperature (K)
<b>U</b> ( <i>u, v, w</i> )	velocity vector with its components (m/s)
<b>X</b> ( <i>x, y, z</i> )	position vector in Cartesian coordinates (m)
<b>Greek symbols</b>	
<i>α</i>	thermal diffusivity (m <sup>2</sup> /s)
<i>β</i>	volumetric thermal expansion coefficient (1/K)
<i>φ</i>	tilt angle from horizontal (°)
<i>μ</i>	viscosity (kg/m.s)
<i>ν</i>	kinematic viscosity (m <sup>2</sup> /s)
<i>ρ</i>	density (kg/m <sup>3</sup> )
<i>ω</i>	vorticity (1/s)
<b>Subscript</b>	
cr	critical
<b>Superscript</b>	
*	dimensionless (variable)
•	zero contribution if negative (value)

## 1. Introduction

Rayleigh-Benard hydrodynamical instability occurs due to adverse density gradient in a horizontal rectangular channel heated from below. If the Rayleigh number ( $Ra$ ) is above the critical value,  $Ra_{cr}$ , convection cells form. When the channel is tilted from the horizontal with a positive angle, the cell formation changes and an upward flow starts. The flow structure and the formation of the cells in the transverse direction depend on the working fluid, the aspect ratio of the channel, the tilt angle and the Rayleigh number. The major changes in the flow structure occur at certain tilt angles that can be named as the critical tilt angles.

Critical tilt angles are usually defined and obtained for rectangular enclosures. Most of the related studies in the heat transfer literature are for solar collector enclosure cavities in which heat transfer is from the hot collector surface to the glass cover via natural convection when the sides of the enclosure are insulated. For an enclosure that is horizontal or tilted from the horizontal with a small angle, convection rolls (Rayleigh-Benard Cells) form. When the tilt angle is increased, a transition from rolls to a single cell occurs at the critical tilt angle which depends on the aspect ratio of the rectangular enclosure. For higher tilt angles, there is a large single cell. The maximum heat transfer occurs at the smaller angles because of the tight alignment of the convection rolls. When the tilt angle is increased, spanwise ( $z$ -direction) convection rolls become dominant and the streamwise ( $x$ -direction) rolls start to break down. This decreases the heat transfer and at some tilt angle, minimum Nusselt number ( $Nu$ ) occurs. At this point, spanwise convection rolls start to rotate their axes by  $90^\circ$  to the direction of  $z$ -axis. Finally, these cells merge to a single two dimensional roll with its axis in the  $z$ -direction. The critical tilt angle is the angle where the flow mode transition occurs. For air in a rectangular cross section enclosure, the critical tilt angle versus the aspect ratio (Height/Length) is given in Table 1 [1].

In a channel between two infinite parallel plates (parallel plate channel) that is uniformly heated from below, similar convection rolls form for the horizontal channel case. When the channel is tilted from the horizontal, due to buoyancy, a streamwise flow starts. Even at small tilt angles, the regular cell structure breaks down. Longitudinal vortices form and the flow may become unsteady. Heat transfer from the heated bottom plate as well as the velocity distribution of the fluid in the channel depends on  $Ra$  and the tilt angle as in the tilted rectangular enclosure case. The objective of this study is to investigate  $Ra$  and tilt angle dependence for parallel plate channels and to determine whether there are angles at which significant changes in the flow structure occur that we can refer to as critical tilt angles.

Tilted channels in various cross sectional geometries and tilted pipes are used in many different engineering applications. They are especially suitable for creating flow or circulation without using turbo machines. The channel configuration discussed here may also be useful for cooling photovoltaic (PV) solar panels to increase their efficiency by decreasing their surface temperature and using the heated fluid to extract some part of the solar energy that can not be absorbed by the PV panels. These practical applications as well as the need for better understanding the phenomenon are the motivations for performing the present numerical investigation.

## 2. Related Works

The natural convection flow in inclined fluid layers has been investigated both experimentally and numerically by many researchers, focusing on various aspects of the phenomenon. Among them, especially the experimental results in Hollands *et al.* [2] are well accepted and cited in most heat transfer books such as Incropera *et al.* [1]. Hollands *et al.* [2] analyzed inclined air layers in enclosures heated from below with high aspect ratios that have constant prescribed wall temperatures. They experimentally investigated the ranges of  $1708 \leq Ra \cdot \cos \varphi \leq 5 \times 10^4$  and  $15^\circ \leq \varphi \leq 60^\circ$  and obtained two correlations for the average Nu:

$$\overline{Nu} = 1 + 1.44 \left[ 1 - \frac{1708}{Ra \cos \varphi} \right]^* \left( 1 - \frac{(\sin 1.8\varphi)^{1.6} 1708}{Ra \cos \varphi} \right) + \left[ \left( \frac{Ra \cos \varphi}{5830} \right)^{1/3} - 1 \right]^* \quad (1)$$

and

$$\overline{Nu} = 1 + 1.44 \left[ 1 - \frac{1708}{Ra \cos \varphi} \right]^* + \left[ \left( \frac{Ra \cos \varphi}{5830} \right)^{1/3} - 1 \right]^* \quad (2)$$

where  $[ \ ]^*$  is defined as  $[X]^* = (|X| + X) / 2$ . Therefore, there is no contribution if the quantity in the brackets with “\*” is negative. In the present study, equations (1) and (2) are used for comparison.

The experimental studies in literature are recently reviewed in detail by Henderson *et al.* [3] with the motivation of applying and extending them for an integrated collector storage solar water heater. They examined the literature for inclined enclosures of any aspect ratio that is heated from either below or above and presented their review in the form of a table covering the last five decades. Their observations about the findings of the previous studies agree with the observations made during the literature survey of the present study that can be itemized as:

- All studies were performed for a small number of tilt angles [2-9]. For example, ElSherbiny *et al.* [4] investigated  $0^\circ, 15^\circ, 30^\circ, 45^\circ, 60^\circ, 70^\circ, 80^\circ$  and  $90^\circ$  tilt angles while Ruth *et al.* [5] investigated only  $0^\circ$ - $30^\circ$  range.
- For small aspect ratios, Nu depends on the aspect ratio strongly [6].
- For large aspect ratios, the aspect ratio dependence of Nu is weak [2][4][7].
- While going from horizontal to vertical, there are mode transitions corresponding to the maximum and the minimum of Nu (among others especially in [4] and [6]).
- In all experimental studies, at the steady range of angles (usually  $15^\circ$ - $60^\circ$  for large aspect channels), longitudinal vortices were observed. While most of the studies were for air, Azevedo and Sparrow [8] observed longitudinal vortices for water.

Even when experimental studies were performed to determine the critical angles (e.g. in [5]), only rough upper or lower limits were presented, due to experimental difficulties to exactly capture these angles at which flow mode transitions occur.

Since the governing equations and numerical solution methods are well established, numerical studies may be useful in resolving the flow mode transitions and visualizing the resulting flow structures. The numerical studies in the literature do not correspond to the case investigated in the present study, but for the sake of completeness, especially the ones that are related to the experimental works in literature are discussed below.

Yang and Zhu [10] performed a 2-D direct numerical simulation and compared their results with the experimental result of [8]. They confirmed that for water ( $Pr \approx 5$ ), and for tilt angle range of  $45-90^\circ$ ,  $\overline{Nu}$  is a monotonic function of  $Ra \cdot (\text{width/height}) \cdot \sin\phi$ . There are many 2-D numerical studies that investigated natural convection in similar geometries. However, Kasapoglu [11], by comparing 2-D and 3-D simulation results, showed that 2-D simulations are not adequate for numerically studying inclined parallel plate channels heated from below, because they can not resolve the longitudinal vortices that dominate the flow field which are 3-D structures.

There are also few 3-D numerical investigations. Two of them are by Ozoe *et al.* [12][13]. In [12], a tilted rectangular enclosure that was heated from below was investigated using a finite difference approach for the  $Pr=10$  and  $Ra=4000$  case. In [13], an inclined three dimensional square channel was investigated and it was observed that  $\overline{Nu}$  first decreases with the increasing tilt angle, and later increases due to the improved and developed rate of circulation of the single 2-D roll. Both of these studies were performed for exploring the different flow structures at a small number of different angles. Baskaya *et al.* [14] studied the effects of the plate spacing and the tilt angle on natural convection between asymmetrically heated vertical and inclined parallel plates by using a commercial computational code, PHOENICS. The same tilt angles in [9] that are  $45^\circ$ ,  $60^\circ$  and  $90^\circ$  were considered.

Henderson *et al.* [3] also reached to the conclusion that 2-D numerical studies can only be useful for angles close to the vertical ( $70-90^\circ$  range) for which there is a single convection role. The numerical part of their work was also 3-D but only covers seven tilt angles in  $0^\circ-90^\circ$  range with  $15^\circ$  increments.

In the present study, to fill the gap in the literature, the tilt angle dependence is studied rigorously by covering critical ranges of tilt angles with one degree increments. Furthermore, to be able to adequately resolve the flow field, a 3-D numerical scheme with very high accuracy is used.

### 3. Modeling details

The considered parallel plate channel is modeled as a channel between two parallel plates of dimensions  $L_x$  by  $L_z$  that are separated with a distance  $L_y$ , as seen in Fig. 1. The periodical velocity and temperature boundary conditions applied in the  $x$  and  $z$  directions, to make the model to represent an infinite channel. From the numerical analysis view point, the difference between the considered model and a rectangular enclosure with insulated sides is the difference in boundary conditions (BCs), the periodic BC versus the symmetry BC, respectively. The Cartesian coordinate system is placed on the center plane of the channel, thus the channel is between  $-L_y/2$  and  $+L_y/2$  in  $y$  direction.

The top and the bottom plates are at uniform temperatures, the bottom one being higher than the top one. Air is the working fluid with constant properties and with the standard Boussinesq approximation to handle the density variations with the temperature. The simulations are transient starting with zero velocity everywhere as the initial boundary condition. The flow is buoyancy driven and unsteady.

Local and spatially averaged Nusselt numbers on the bottom plate are calculated in order to determine the heat flux from the heated bottom plate at a given time.

### 3.1 Governing equations and boundary conditions

The governing equations are the continuity, the rotational form of the Navier-Stokes equations and the energy equations:

$$\nabla \cdot \mathbf{U} = 0 \quad (3)$$

$$\frac{\partial \mathbf{U}}{\partial t} + \omega \times \mathbf{U} = -\frac{1}{\rho} \nabla p + \nu \nabla^2 \mathbf{U} + \beta \mathbf{g} T \quad (4)$$

$$\frac{\partial T}{\partial t} + \mathbf{U} \cdot \nabla T = \alpha \nabla^2 T \quad (5)$$

where  $\mathbf{U}$  is the velocity vector with  $u$ ,  $v$  and  $w$  components in  $x$ ,  $y$  and  $z$  directions.  $\mathbf{g}$  is the gravitational acceleration vector with the components  $g \sin \varphi$  and  $g \cos \varphi$  in the  $x$  and  $y$  directions for a given tilt angle of  $\varphi$  measured from the horizontal. The fluid properties at temperature  $T$  are  $\alpha$ ,  $\beta$  and  $\nu$ .  $\omega = \nabla \times \mathbf{U}$  is the vorticity. In Eq. (5), viscous dissipation is included for the sake of making the numerical solution general, even though its contribution is negligible for air.

The boundary conditions for the velocity field are:

$$\mathbf{U}(x, y, z, t) = 0 \quad \text{at} \quad y = \pm L_y / 2 \quad (\text{No slip condition})$$

$$\mathbf{U}(x + mL_x, y, z + nL_z, t) = \mathbf{U}(x, y, z, t) \quad (\text{Periodic condition})$$

where  $m$  and  $n$  are integers. The boundary conditions for the temperature field are:

$$T(x + mL_x, y, z + nL_z, t) = T(x, y, z, t) \quad (\text{Periodic Condition})$$

$$T(x, y, z, t) = T_1(x, z) \quad \text{at} \quad y = -L_y / 2$$

$$T(x, y, z, t) = T_2(x, z) \quad \text{at} \quad y = +L_y / 2$$

In order to determine the non-dimensional form of Eqns. (3-5),  $\bar{U}$  and  $\bar{L}$  are used as the characteristic velocity and length scales of the problem, respectively. The half channel height,  $L_y/2$  is used as the length scale. Since the flow is buoyancy driven natural convection flow, to get rid of  $Re$  in the dimensionless form of the governing equations, the characteristic velocity is selected as  $\bar{U} = \alpha / \bar{L}$ . Temperature is non-dimensionalized by using the maximum temperature difference  $\Delta T = T_1 - T_2$ . By describing the dimensionless parameters with the superscript “\*”, the relations between the non-dimensional and the dimensional parameters are:

$$\mathbf{U}^* = \frac{\mathbf{U}}{\bar{U}}, \quad \mathbf{X}^* = \frac{\mathbf{X}}{\bar{L}}, \quad t^* = \frac{\bar{U}}{\bar{L}} t, \quad \theta^* = \frac{T - T_1}{\Delta T}, \quad p^* = \frac{p}{\rho \bar{U}^2}.$$

Eqns. (3-5) take the form:

$$\nabla \cdot \mathbf{U}^* = 0 \quad (6)$$

$$\frac{\partial \mathbf{U}^*}{\partial t^*} + \omega^* \times \mathbf{U}^* = -\nabla p^* + Pr \nabla^2 \mathbf{U}^* + Ra Pr \theta^* \frac{\mathbf{g}}{g} \quad (7)$$

$$\frac{\partial \theta^*}{\partial t^*} + \mathbf{U}^* \cdot \nabla \theta^* = \nabla^2 \theta^* \quad (8)$$

where  $Ra = \frac{\bar{L}^3 \beta g \Delta T}{\alpha \nu}$ , and  $Pr = \frac{\nu}{\alpha}$ . While discussing the results, following the convention,  $Ra$  is presented based on the channel height, thus  $Ra$  is multiplied with  $2^3=8$ .

### 3.2 Solution method

A spectral method based approach is used in the solution of the dimensionless form of the governing equations.  $U^*$  and  $\theta^*$  are expanded to Fourier series in the streamwise and the spanwise directions and to Chebyshev polynomials in the normal direction. In the spatial discretization, with the choice of Gauss-Lobatto-Chebyshev points in the normal direction, real Fast Fourier Transform (FFT) is used to go forward and backward between Fourier-Chebyshev and physical spaces. For convenience, the range of the computational domain in the  $x$  and  $z$  directions (where the solution is periodical) are taken from 0 to  $2\pi$  (a single period). A detailed discussion of spectral methods as well as the polynomial expansions can be found in Peyret [15].

Differentiations and integrations are performed in the Fourier-Chebyshev space while arithmetic operations are performed in the physical space. Therefore; the method requires many forward and backward FFTs per time step which makes it computationally expensive.

The method has the advantage of so called spectral accuracy. With the increasing polynomial order, the accuracy of the global solution surpasses the accuracy that can be obtained by finite difference and finite element approaches. This kind of high accuracy is especially needed for the flows where inherent physical instabilities dominate the solution such as the phenomenon that is investigated in the present study.

One should note that there is no h-type refinement here, therefore, when a finer mesh is used, only the polynomial order of the global solution increases (p-type refinement). Due to this fact, the highest possible polynomial order (mesh size) is desired. Therefore, there is no need for a conventional grid independency check. Considering the available computational resources, one selects the highest possible mesh size that gives feasible simulation runtimes. In an event that is dominated by diffusion, the time scale is the diffusion time scale. Hence, an increase in mesh size requires a decrease in the time step size which makes simulations to run longer. Here, the selected mesh that gives reasonable simulation runtimes is  $32 \times 64 \times 32$  with a higher resolution in  $y$ -direction.

For temporal discretization, after trying Adams-Bashforth / Crank-Nicolson (ABCN) and Adams-Bashforth / 2nd Order Backward-Differencing (ABBDI2), as the semi implicit discretization scheme, Modified ABCN (MABCN) is selected for being the most stable one among the three. Details of these schemes can be found in [15] and [16]. For all of the three schemes, the  $u$ -velocity component versus dimensionless time at the center of the domain for  $Ra=20000$ ,  $\varphi=15^\circ$  and  $dt^* = 10^{-4}$  is shown in Fig. 2. For MABCN, it is observed that due to the relatively high  $Ra$ , oscillations remain even after  $t^*=60$  which is a dimensionless time value at which a steady flow mode is observed for all of the  $Ra$  values that are examined in the present study. These oscillations are the motion of the formed longitudinal vortices in all three dimensions. When other semi implicit schemes used, the oscillations were much severe for the same case. Especially, ABCN scheme leads to results that are not converged.

### 3.3 Nusselt number calculation

After obtaining the temperature field, to compare the results with the ones in literature and to be able to determine the critical tilt angles, space averaged Nu,  $\overline{Nu}$ , should be calculated at the time where steady state is reached.

At steady state, the local energy balance on the lower plate is:

$$-k \left. \frac{\partial T}{\partial y} \right|_{y=-L_y/2} = h(T_1 - T_\infty) \quad (9)$$

where  $k$  is the thermal conductivity of the fluid,  $h$  is the local heat transfer coefficient of the fluid,  $T_1$  is the local wall temperature of the lower plate,  $T_\infty$  is the mean temperature of the fluid. The temperature gradient term on the left hand side is local, and it is calculated for every  $x$  and  $z$  locations. Local Nu can be written as:

$$Nu = \frac{hL_y}{k} = \frac{-L_y \left. \frac{\partial T}{\partial y} \right|_{y=-L_y/2}}{T_1 - T_\infty} \quad (10)$$

Eqn. (10) can be non-dimensionalized, as follows:

$$Nu = \frac{- \left. \frac{\partial \theta^*}{\partial y^*} \right|_{y^*=-1}}{(\theta_1^* - \theta_\infty^*)} \quad (11)$$

The temperature gradient term in Eqn. (11) can be approximated as,

$$\left. \frac{\partial \theta^*}{\partial y^*} \right|_{y^*=-1} \cong \frac{\Delta \theta^*}{\Delta y^*} \Big|_{y^*=-1} \quad (12)$$

where  $\Delta y^*$  is the distance between the lowermost collocation points.  $\theta_\infty^*$  is calculated by taking the mean of each  $\theta^*$  value of the fluid in  $y$  direction. To obtain  $\overline{Nu}$ , the average over all  $x$  and  $z$  locations is calculated.

## 4. Results and discussions

The phenomenon investigated here is an unsteady one, however, depending on Ra and  $\varphi$ , it reaches to a mode that is either steady or steadily oscillating. To characterize the steady mode, time change of  $\overline{Nu}$  is examined. Especially at high Ra, it becomes harder to resolve the steadily oscillating flow mode in a reasonable simulation runtime, due to very small time step size requirements. Therefore; when simulations are performed for a fixed Ra or  $Ra \cdot \cos \varphi$ , relatively small constant values are selected. The critical tilt angle ( $\varphi_{cr}$ ) term is used for the tilt angle where a significant change occurs in the flow structure.

The steady mode of the flow is obtained after certain periods of time depending on Ra and  $\varphi$ . The steady mode can be either a steady state or a state at which a steady flow structure moves steadily in the domain creating steady oscillations in the flow variables. In Figs 3 and 4, the variations of local Nu over time in the streamwise and spanwise directions are given for two different cases. Figure 3 is for  $Ra=7000$  case with  $\varphi=50^\circ$  which reaches a steady state. Fig. 4 is for  $Ra \cdot \cos \varphi=10000$  case with  $\varphi=15^\circ$  which

reaches to a steadily oscillating mode at  $t^*=10$ . The local Nu distribution in the  $z$ -direction at  $t^*=8$  and 10 exactly coincide, indicating that the longitudinal vortex structure is steady. However, in the  $x$ -direction the distribution shifts to the right with a constant speed, causing oscillations in all velocity components.

The velocity and temperature fields at the center planes of the domain for  $Ra=10000$ ,  $\varphi=50$  case at  $t^*=30$  are shown in Fig. 5. To visualize the 3-D velocity field  $\int udy$  is used for being similar to stream function in 2-D. The plumes and the resulting longitudinal vortices are apparent, especially in the  $z$ - $y$  views.

After reaching a steady mode, the change of  $\overline{Nu}$  with  $Ra \cdot \cos\varphi$  for the fixed tilt angle of  $15^\circ$  is shown in Fig. 6. In this figure, the correlation results from Eqns. (1) and (2) are also shown. The present results agree well with the correlation results.

To determine the critical tilt angles and to compare the results with Eqns. (1) and (2), one needs to fix either the  $Ra$  or the  $Ra \cdot \cos\varphi$  and to observe the change of  $\overline{Nu}$  with  $\varphi$ . Eq. (1) is the Hollands *et al.* [2] correlation that gives  $\overline{Nu}$  as a function of  $Ra \cdot \cos\varphi$  and  $\varphi$ . Eq. (2) is their simplified correlation that gives  $\overline{Nu}$  as a function of  $Ra \cdot \cos\varphi$  only.

As the first case:  $Ra \cdot \cos\varphi$  is fixed to 3500 which is above  $Ra_{cr}$ , but also small enough to reach convergence within an acceptably low simulation runtime. For this case,  $\overline{Nu}$  versus  $\varphi$  results are plotted in Fig. 7 together with the Hollands *et al.* [2] correlation results. It is observed that in the range that the correlations are valid ( $15$ - $60^\circ$  range), the present simulation results are constant at  $\overline{Nu}=1.6776$  while Eq. (2) also gives a constant value at  $\overline{Nu}=1.7373$ . The simulation results are bounded with Eq. (1) and Eq. (2) results. However, since Eq. (1) does not give a constant value, it does not seem to be in agreement with the simulation results. From the figure, it is also obvious that the range of correlations is actually the range that the flow is steady. There are no flow mode changes in that range. Immediately below  $15^\circ$  and above  $60^\circ$ , the trends of  $\overline{Nu}$  are different. At around  $12^\circ$ , a local minimum of  $\overline{Nu}$  occurs which is 1.3892 that corresponds to a steadily oscillating mode. In fact, all of the modes below  $15^\circ$  and above  $60^\circ$  are oscillating modes. The maximum occurs at  $\varphi = 72^\circ$  as  $\overline{Nu}=2.1252$ . Right after that maximum, a sharp decrease in  $\overline{Nu}$  is observed. According to Fig. 7, in a parallel plate channel (infinite aspect ratio), the critical tilt angles for air are  $12^\circ$  and  $72^\circ$ . The error bars correspond to one standard deviation of spatially averaged Nu in the time period that is considered to calculate  $\overline{Nu}$  which is  $20 < t^* \leq 30$ . As it can be seen there is no deviation in  $15^\circ \leq \varphi \leq 60^\circ$ . Outside of this range, there are deviations due to oscillations of the cell structures. These oscillations are especially severe around the mode transitions. With the accuracy achieved in the numerical approach of the present study, these regions of interest are successfully resolved.

In Fig. 8, for  $Ra \cdot \cos\varphi = 3500$  case, the velocity fields at the center planes of the domain are shown at  $\varphi = 50^\circ$  (top),  $72^\circ$  (middle) and  $73^\circ$  (bottom).  $50^\circ$  is within the steady range where everything is quiet and the  $z$ - $y$  view shows that there are developed steady longitudinal vortices. At  $72^\circ$ , the maximum  $\overline{Nu}$  occurs followed by a sudden drop at  $73^\circ$ . The flow structures oscillate at both of these angles, the plots are frozen at  $t^*=30$ . It is not obvious from the center plane results, but at  $72^\circ$ , the flow is stronger.

As the second case: Ra is fixed to 7000 which is low enough for fast convergence. In Fig. 9, again  $\overline{Nu}$  versus  $\varphi$  results are plotted together with the Hollands *et al.* [2] correlation results. Here,  $Ra \cdot \cos\varphi$  drops below  $Ra_{cr}$  for angles above  $76^\circ$ . The heat transfer mode for higher angles is conduction. When the range of Hollands *et al.* [2] correlations examined, it is observed that the data shows a better agreement with Eq. (2), but the third order polynomial fit seems more appropriate than the linear fit. In  $17^\circ \leq \varphi \leq 60^\circ$  range, for the third order polynomial fit, the coefficient of determination,  $R^2$  is 0.98 compared to 0.82 for the linear fit. The resulting correlation is:

$$\overline{Nu} = -2 \times 10^{-5} \varphi^3 + 0.0026 \varphi^2 - 0.0942 \varphi + 3.1172 \quad (13)$$

Here, the critical tilt angles appear to be  $17^\circ$  and  $73^\circ$ . At  $17^\circ$ , the maximum value of  $\overline{Nu}$  is observed while at  $73^\circ$ , there is a sudden drop in  $\overline{Nu}$ .

For the third set of simulations, Ra is fixed at 10000, and Fig. 10 is obtained. Again the third order polynomial fit is the appropriate fit. In  $15^\circ \leq \varphi \leq 60^\circ$  range, for the third order polynomial fit,  $R^2$  is 0.95 compared to 0.57 for the linear fit. Thus, the observed correlation is:

$$\overline{Nu} = -3 \times 10^{-5} \varphi^3 + 0.0033 \varphi^2 - 0.1127 \varphi + 3.4149 \quad (14)$$

From Ra=10000 data, the critical tilt angles are obtained as  $14^\circ$  and  $76^\circ$ .

In Fig. 11, which is for Ra= 10000 case, the velocity fields at the center planes of the domain are shown at  $\varphi = 14^\circ$  (top),  $50^\circ$  (middle) and  $76^\circ$  (bottom). Again,  $50^\circ$  is within the steady range where everything is quiet and the  $z$ - $y$  view shows that there are developed steady longitudinal vortices. At  $14^\circ$ , the maximum  $\overline{Nu}$  and at  $76^\circ$ , the minimum  $\overline{Nu}$  occur. The flow structures oscillate at  $76^\circ$  but steady and strong at  $14^\circ$ .

Hollands *et al.* [2] correlates  $\overline{Nu}$  with  $Ra \cdot \cos\varphi$ . Following that approach, the data from Ra=7000 and Ra=10000 cases are combined and analyzed together. The resulting  $\overline{Nu}$  versus  $Ra \cdot \cos\varphi$  plot is presented together with the results from Eq. (2) in Fig. 12. The present fit is obtained by assuming the same form as Eq. (2) and using the non-linear fit. The present fit equation is:

$$\overline{Nu} = 1 + 1.4884 \left[ 1 - \frac{1708}{Ra \cos \varphi} \right] + \left[ \left( \frac{Ra \cos \varphi}{5830} \right)^{1/9.3359} - 1 \right] \quad (15)$$

In Fig. 12, if the data for Ra=7000 and Ra=10000 are separately analyzed, the third order polynomial fit results of Figures 9 and 10 are obtained. The difference between Hollands *et al.* [2] correlation, Eq. (2) and the present one may be due to the difference in the geometry, namely between a large aspect ratio enclosure and a parallel plate channel. The better fit of third order polynomials for the separate Ra cases is an indication of dependence of  $\overline{Nu}$  to  $Ra \cdot \cos\varphi$  and Ra itself. In this case, a form involving also a separate Ra related term may be more appropriate for the data fit. It is also observed that Eq. (1) which involves a separate  $\varphi$  related term can not be used for data fit at least for Ra=7000 and 10000 values.

The obtained critical tilt angle values for air show that they weakly depend on Ra or  $Ra \cdot \cos\varphi$ , but for the cases considered, it can be said that, one of them is around  $15^\circ$  and the other one is around  $74^\circ$ . For enclosures with large aspect ratios, the critical tilt angle value cited in the literature is  $70^\circ$ . Considering that the present simulations are limited to the three separate cases, due to prohibiting runtime and data storage requirements, the agreement seems to be acceptable. One should also note that an experimental study

trying to determine critical tilt angles faces with the same problems, namely critical tilt angles correspond to flow mode transitions where the measurements related to flow characteristics are very difficult to perform; therefore, the experimentally determined value may also have a large error associated with it. There is a single value of  $70^\circ$  that is cited for large aspect ratios, Table 1 shows that the value for the infinite aspect ratio may be higher than that, considering the increasing trend of  $\varphi_{cr}$  with the aspect ratio.

## 5. Conclusions

The simulations performed in this study were successful in resolving the flow and temperature fields in an inclined parallel plate channel heated from below. After reaching a steady mode,  $\overline{Nu}$  values were calculated and their dependencies on  $Ra$ ,  $Ra \cdot \cos\varphi$  and  $\varphi$  were investigated.

In the  $15^\circ \leq \varphi \leq 60^\circ$  range where Hollands *et al.* [2] correlations are valid, there is a good agreement with them, especially with Eq. (2). When  $Ra$  is kept constant, for each  $Ra$ , a different third order polynomial fit between  $\overline{Nu}$  and  $\varphi$  is obtained, suggesting that a separate  $Ra$  dependence may be present.

Outside of  $15^\circ \leq \varphi \leq 60^\circ$  range, oscillations of the cell structures are observed to be especially severe around the mode transitions. With the accuracy achieved in the numerical approach of the present study, these regions of interest are successfully resolved. It is observed that all of the interesting changes in flow structure occur outside of the steady range. The lower bound of this range ( $\sim 15^\circ$ ) appears to be the point where a mode transition occurs and it corresponds to the maximum  $\overline{Nu}$  values in the constant  $Ra$  simulations and the local minima in the constant  $Ra \cdot \cos\varphi$  simulations.

Around  $74^\circ$ , another transition occurs which corresponds to the maximum  $\overline{Nu}$  values in the constant  $Ra \cdot \cos\varphi$  simulations and the local minima in the constant  $Ra$  simulations. For the considered cases, the critical tilt angle values differ slightly suggesting that they depend on  $Ra$  weakly. It may not be possible to give one or two distinct angles as the critical tilt angles for air. However, knowing the critical tilt angles approximately may be enough for the applications (e.g. an inclined channel heat exchanger) requiring the maximum or the minimum possible heat flux.

The common tilt angles for solar panels or roofs are usually within  $30$ - $60^\circ$  range, and neither  $15^\circ$  nor  $74^\circ$  are important angles for these applications. However, for  $30$ - $60^\circ$  range knowing the tilt angle dependence of the heat flux precisely may be important, and the numerical approach of the present study is very precise in that range. Furthermore, with the recently increased demand for solar power, installations started to appear at various latitudes of the world thus widening the range of angles that the panels are tilted.

There are studies in the literature investigating solar panels having rectangular heat sources [17] or corrugated walls [18] for which resulting disturbances dominate the flow field, however the present study is limited to flat and smooth walls with uniform temperatures.

## PREPRINT.

Ilker Tari, "Natural Convection Simulations and Numerical Determination of Critical Tilt Angles for a Parallel Plate Channel," *Energy Conversion and Management*, Vol. 51, No. 4, pp. 685-695 (2010).

## References

- [1] Incropera FP, DeWitt DP, Bergman TL, Lavine AS. *Fundamentals of heat and mass transfer*. 6th ed. Hoboken NJ: John Wiley & Sons; 2007.
- [2] Hollands KGT, Unny TE, Raithby GD, Konicek L. Free convective heat transfer across inclined air layers. *J Heat Trans-T ASME* 1976;98:189–93.
- [3] Henderson D, Junaidi H, Muneer T, Grassie T, Currie J. Experimental and CFD investigation of an ICSSWH at various inclinations. *Renew Sust Energy Rev* 2007;11:1087–116.
- [4] ElSherbiny SM, Raithby GD, Hollands KGT. Heat transfer by natural convection across vertical and inclined air layers. *J Heat Trans-T ASME* 1982;104:96–102.
- [5] Ruth DW, Hollands KGT, Raithby GD. On free convection experiments in inclined air layers heated from below. *J Fluid Mech* 1980;96:461–79.
- [6] Ozoe H, Sayama H, Churchill SW. Natural convection in an inclined rectangular channel at various aspect ratios and angles - Experimental measurements. *Int J Heat Mass Tran* 1975;18:1425–31.
- [7] Inaba H. Experimental study of natural convection in an inclined air layer. *Int J Heat Mass Tran* 1984;27:1127–39.
- [8] Azevedo LFA, Sparrow EM. Natural convection in open-ended inclined channels. *J Heat Trans-T ASME* 1985;107:893–901.
- [9] Onur N, Sivrioglu M, Aktas MK. An experimental study on the natural convection heat transfer between inclined plates (Lower plate isothermally heated and the upper plate thermally insulated as well as unheated). *Heat Mass Transfer* 1997;32:471–6.
- [10] Yang HX, Zhu ZJ. Numerical study on transient laminar natural convection in an inclined parallel-walled channel. *Int Commun Heat Mass* 2003;30:359–67.
- [11] Kasapoglu S. A pseudospectral analysis of laminar natural convection flow and heat transfer between two inclined parallel plates. MS thesis, METU, Ankara, 2005.
- [12] Ozoe H, Fujii K, Lior N, Churchill SW. Long rolls generated by natural convection in an inclined, rectangular enclosure. *Int J Heat Mass Tran* 1983;26:1427–38.
- [13] Ozoe H, Yamamoto K, Churchill SW. Three-dimensional numerical analysis of natural convection in an inclined channel with a square cross section. *AIChE J* 1979;25:709–16.
- [14] Baskaya S, Aktas MK, Onur N. Numerical simulation of the effects of plate separation and inclination on heat transfer in buoyancy driven open channels. *Heat Mass Transfer* 1999;35:273–80.
- [15] Peyret R. *Spectral methods for incompressible viscous flow*. Berlin: Springer-Verlag; 2002.
- [16] Ascher UM, Ruuth SJ, Wetton BTR. Implicit-explicit methods for time-dependent partial differential equations. *SIAM J Numer Anal* 1995;32:797–823.
- [17] Bakkas M, Amahmid A, Hasnaoui M. Steady natural convection in a horizontal channel containing heated rectangular blocks periodically mounted on its lower wall. *Energy Convers Manage* 2006;47:509–28.
- [18] Gao W, Lin W, Lu E. Numerical study on natural convection inside the channel between the flat-plate cover and sine-wave absorber of a cross-corrugated solar air heater. *Energy Convers Manage* 2000;41:145–51.

PREPRINT.

Ilker Tari, "Natural Convection Simulations and Numerical Determination of Critical Tilt Angles for a Parallel Plate Channel," Energy Conversion and Management, Vol. 51, No. 4, pp. 685-695 (2010).

**Table 1** Critical tilt angle ( $\varphi_{cr}$ ) versus aspect ratio ( $H/L$ ) for tilted rectangular enclosures filled with air [1].

$H/L$	1	3	6	12	>12
$\varphi_{cr}$	25°	53°	60°	67°	70°

PREPRINT.

Ilker Tari, "Natural Convection Simulations and Numerical Determination of Critical Tilt Angles for a Parallel Plate Channel," Energy Conversion and Management, Vol. 51, No. 4, pp. 685-695 (2010).

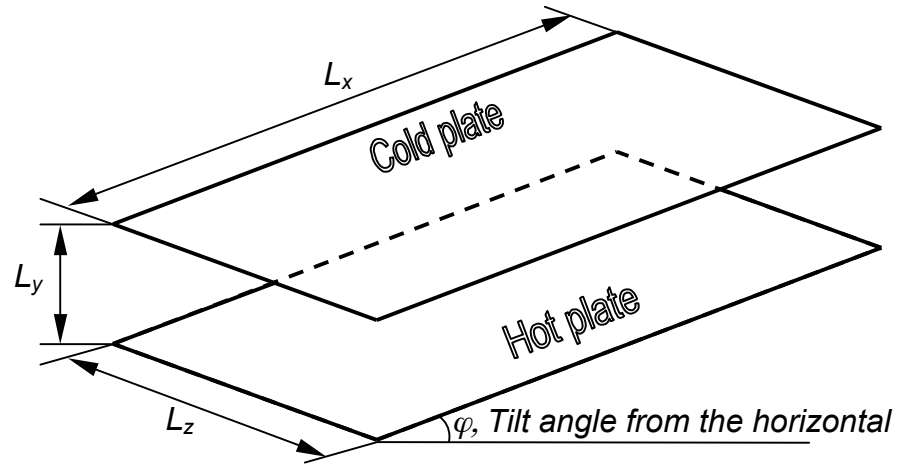


**Fig. 1** Computational domain

PREPRINT.

Ilker Tari, "Natural Convection Simulations and Numerical Determination of Critical Tilt Angles for a Parallel Plate Channel," Energy Conversion and Management, Vol. 51, No. 4, pp. 685-695 (2010).

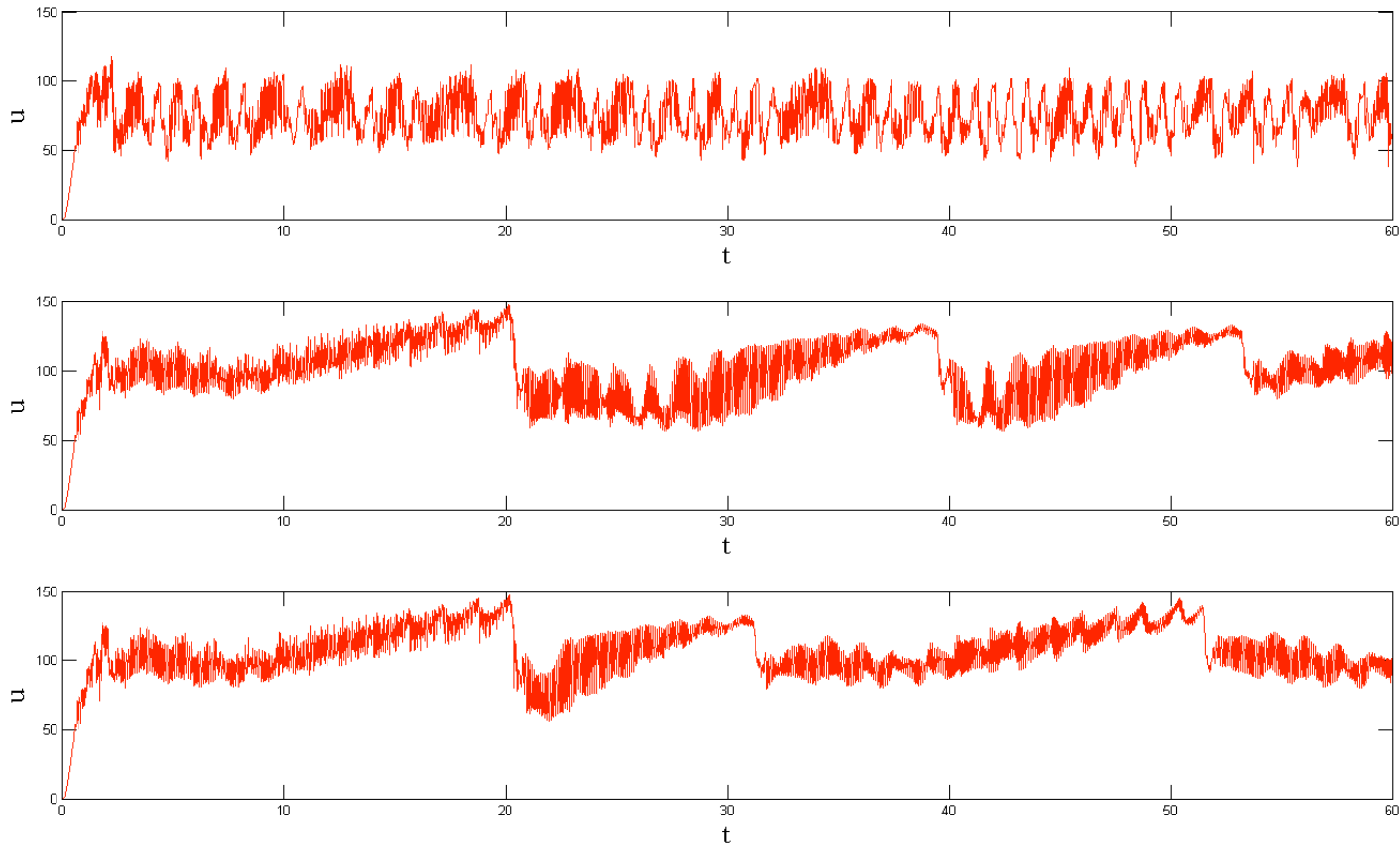


**Fig. 2** Comparison of ABCN (top), ABBDI2 (middle) and MABCN (bottom) semi-implicit schemes, u-velocity components vs time at the domain center for  $Ra= 20000$ ,  $\varphi=15^\circ$  and  $dt = 10^{-4}$

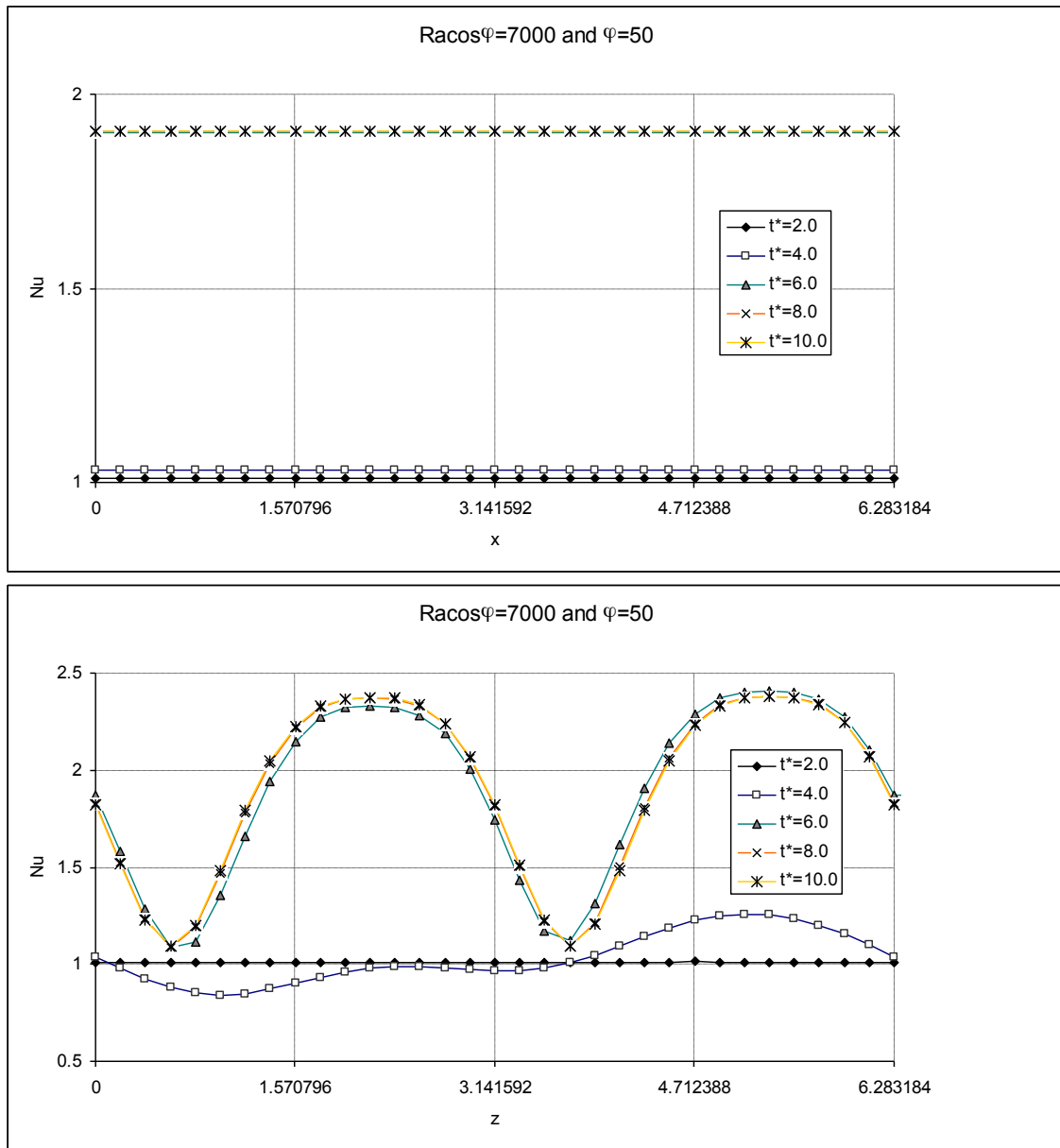


**Fig. 3** Local Nu in streamwise (top) and spanwise (bottom) directions for Ra=7000 and  $\varphi=50^\circ$

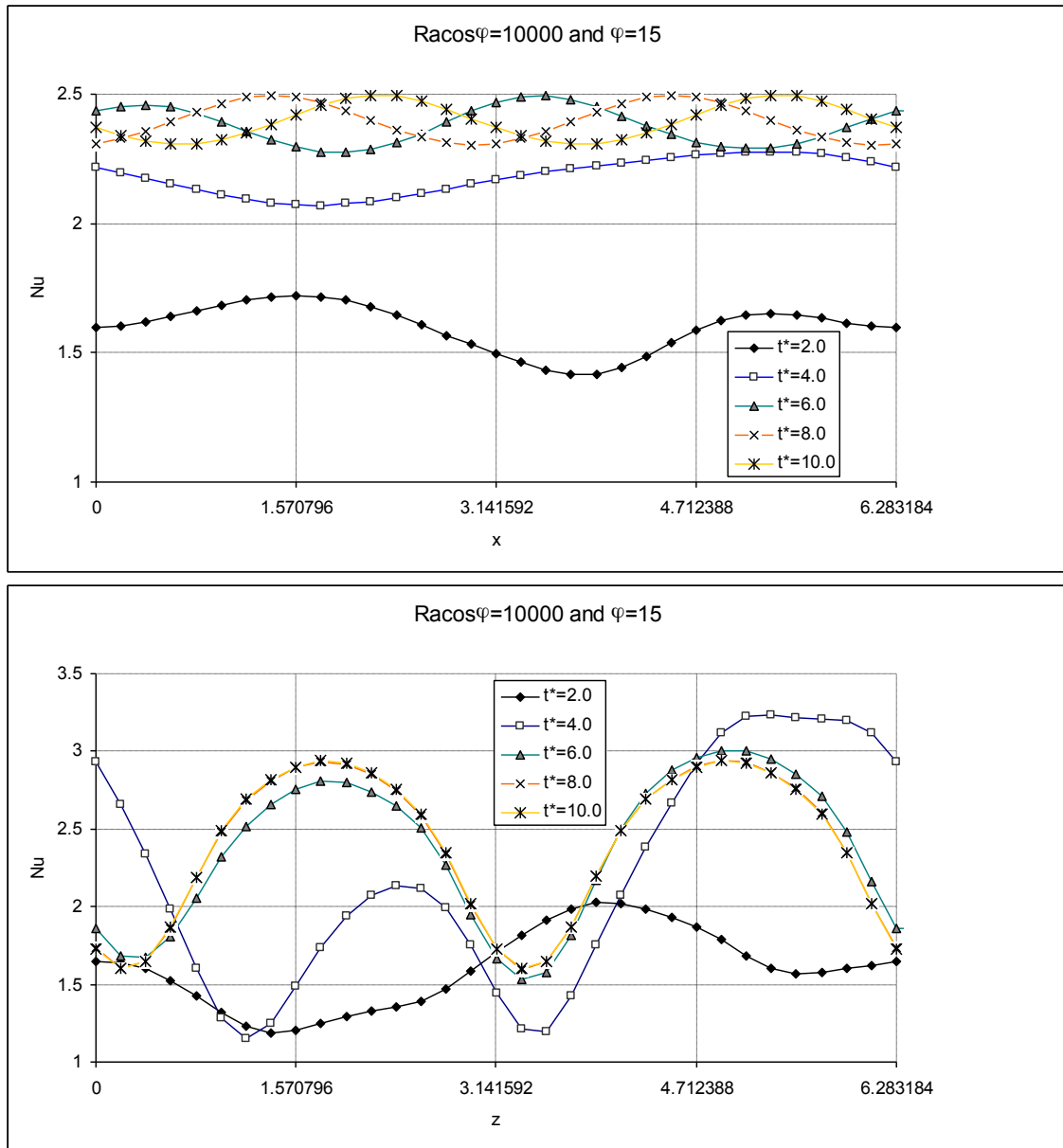


**Fig. 4** Local Nu in streamwise (top) and spanwise (bottom) directions for  $Ra \cdot \cos \varphi = 10000$  and  $\varphi = 15^\circ$

PREPRINT.

Ilker Tari, "Natural Convection Simulations and Numerical Determination of Critical Tilt Angles for a Parallel Plate Channel," Energy Conversion and Management, Vol. 51, No. 4, pp. 685-695 (2010).

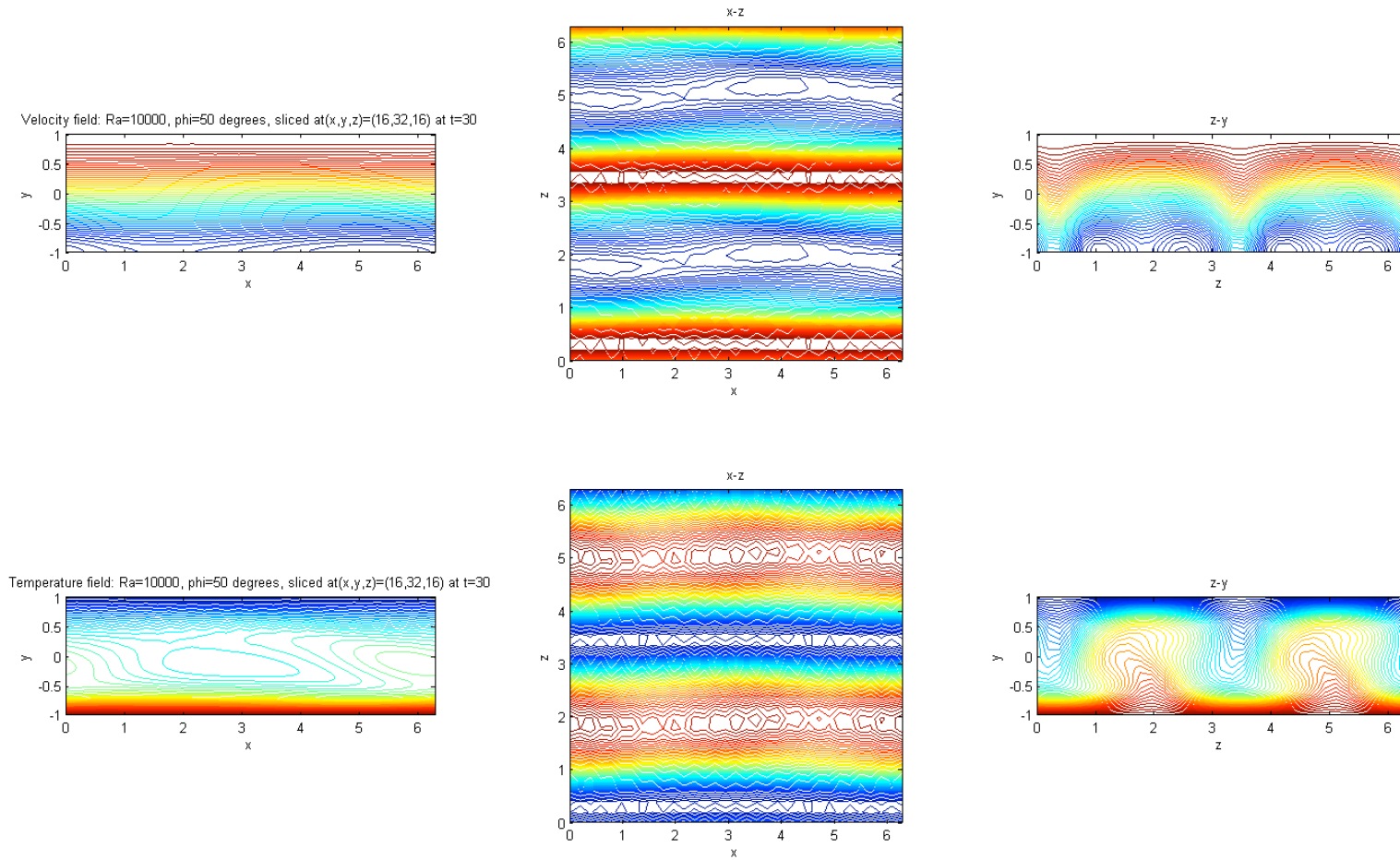


**Fig. 5** Velocity (top) and temperature (bottom) fields at the center planes of the domain for  $Ra=10000$ ,  $\varphi=50$  at  $t^*=30$

PREPRINT.

Ilker Tari, "Natural Convection Simulations and Numerical Determination of Critical Tilt Angles for a Parallel Plate Channel," Energy Conversion and Management, Vol. 51, No. 4, pp. 685-695 (2010).

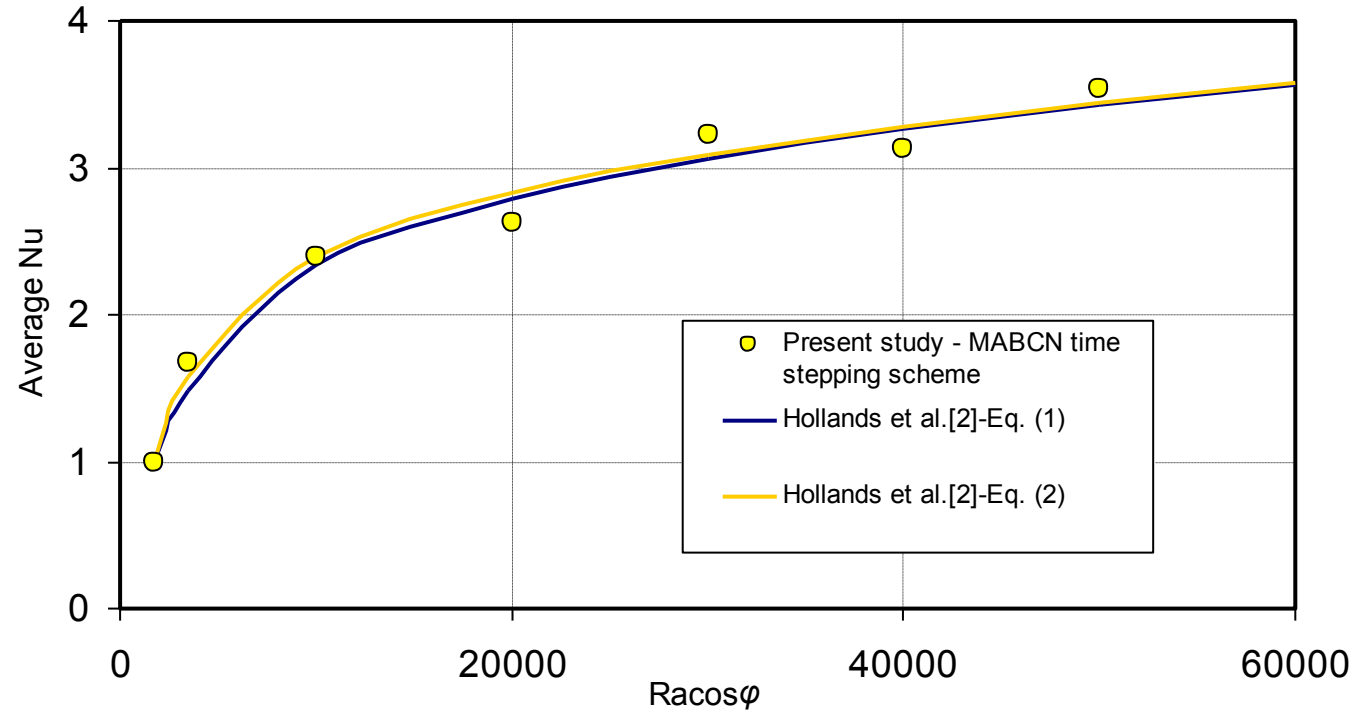


Fig. 6  $\overline{Nu}$  versus  $Ra \cdot \cos \phi$  where  $\phi = 15^\circ$

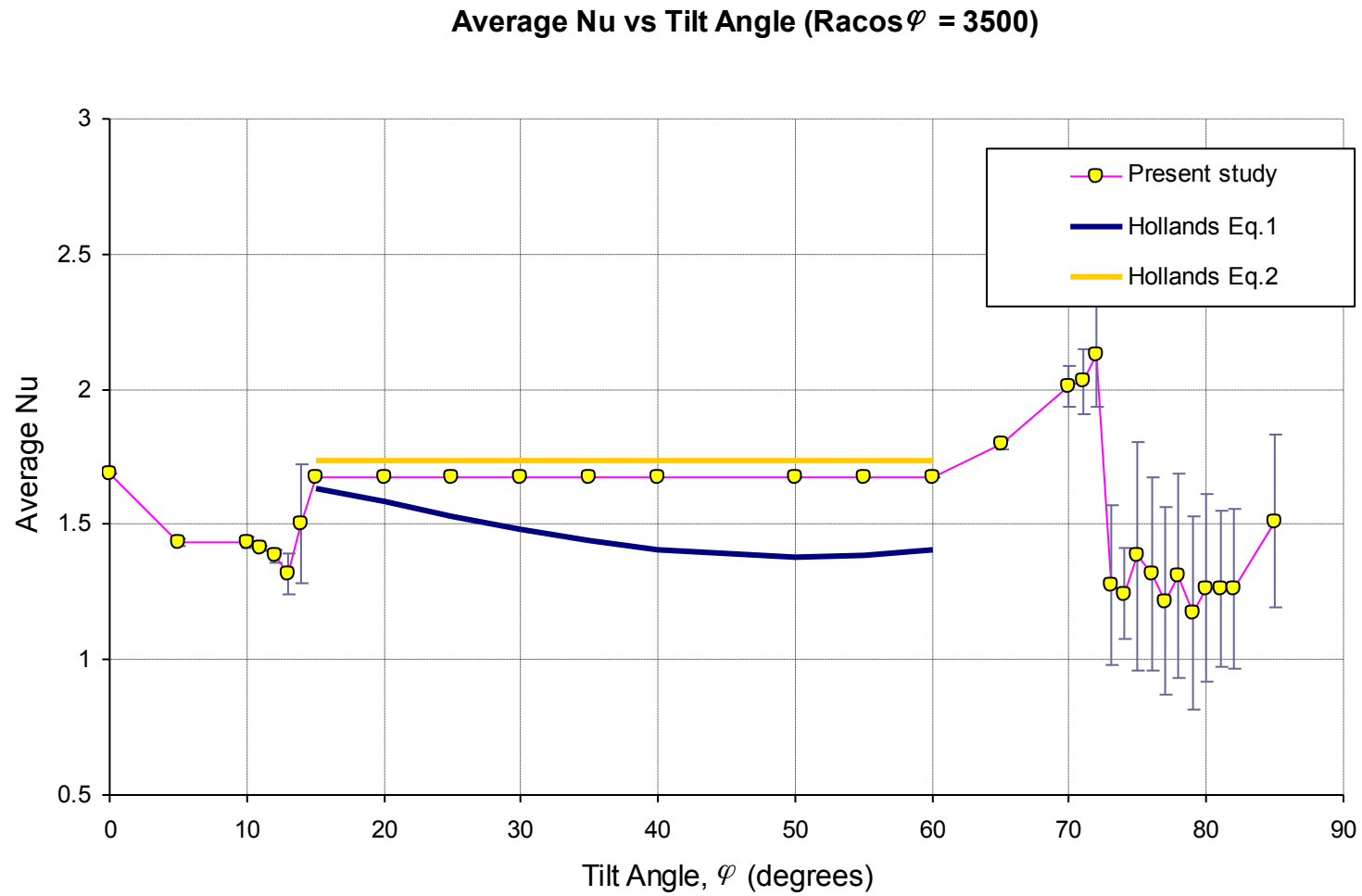
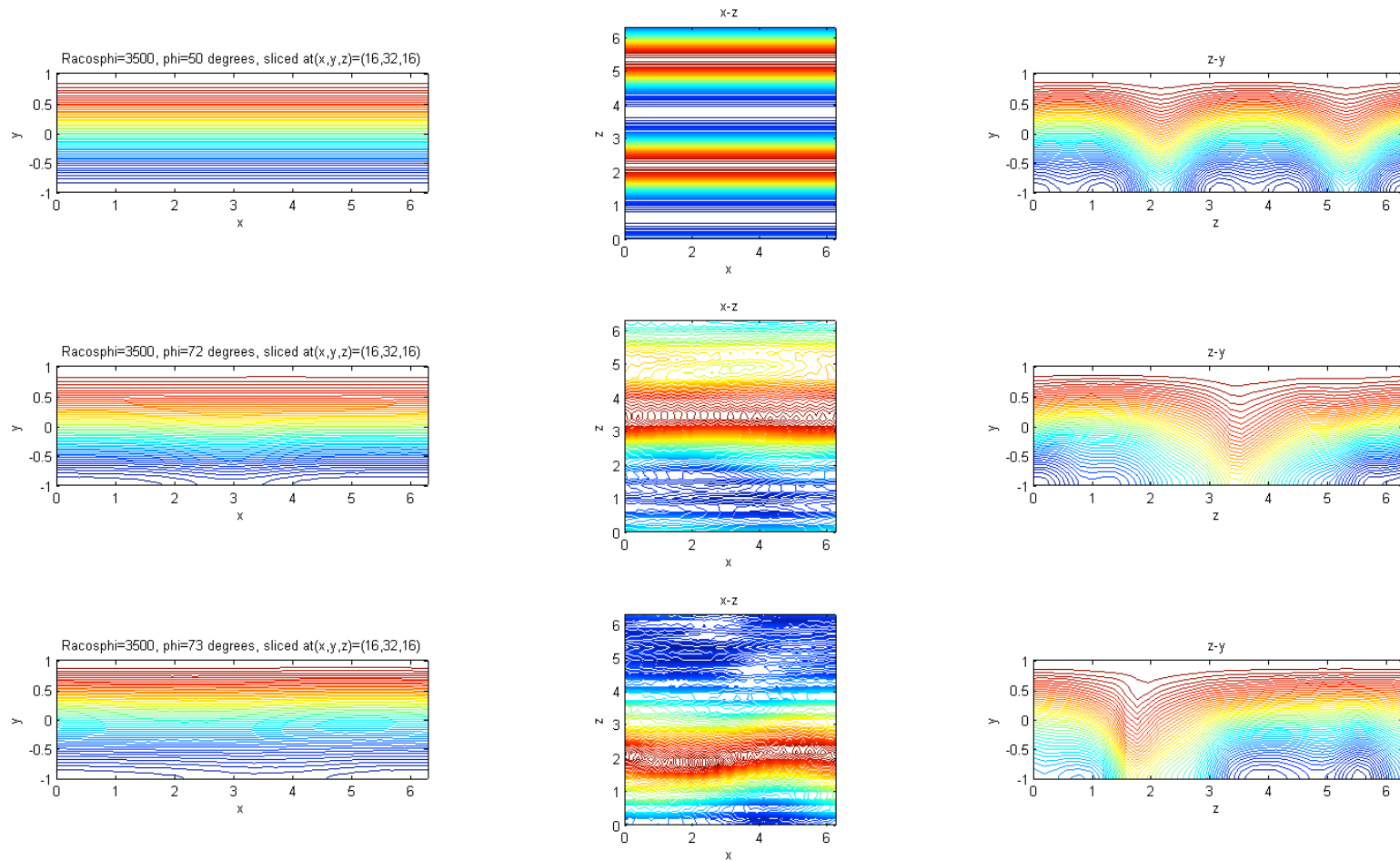


Fig. 7  $\overline{Nu}$  versus  $\varphi$ , for  $Ra \cdot \cos \varphi = 3500$

PREPRINT.

Ilker Tari, "Natural Convection Simulations and Numerical Determination of Critical Tilt Angles for a Parallel Plate Channel," Energy Conversion and Management, Vol. 51, No. 4, pp. 685-695 (2010).



**Fig. 8** Velocity fields for  $Ra \cdot \cos\varphi = 3500$ ,  $\varphi = 50^\circ$  (top),  $72^\circ$  (middle) and  $73^\circ$  (bottom) at  $t^* = 30$ , sliced at the center planes

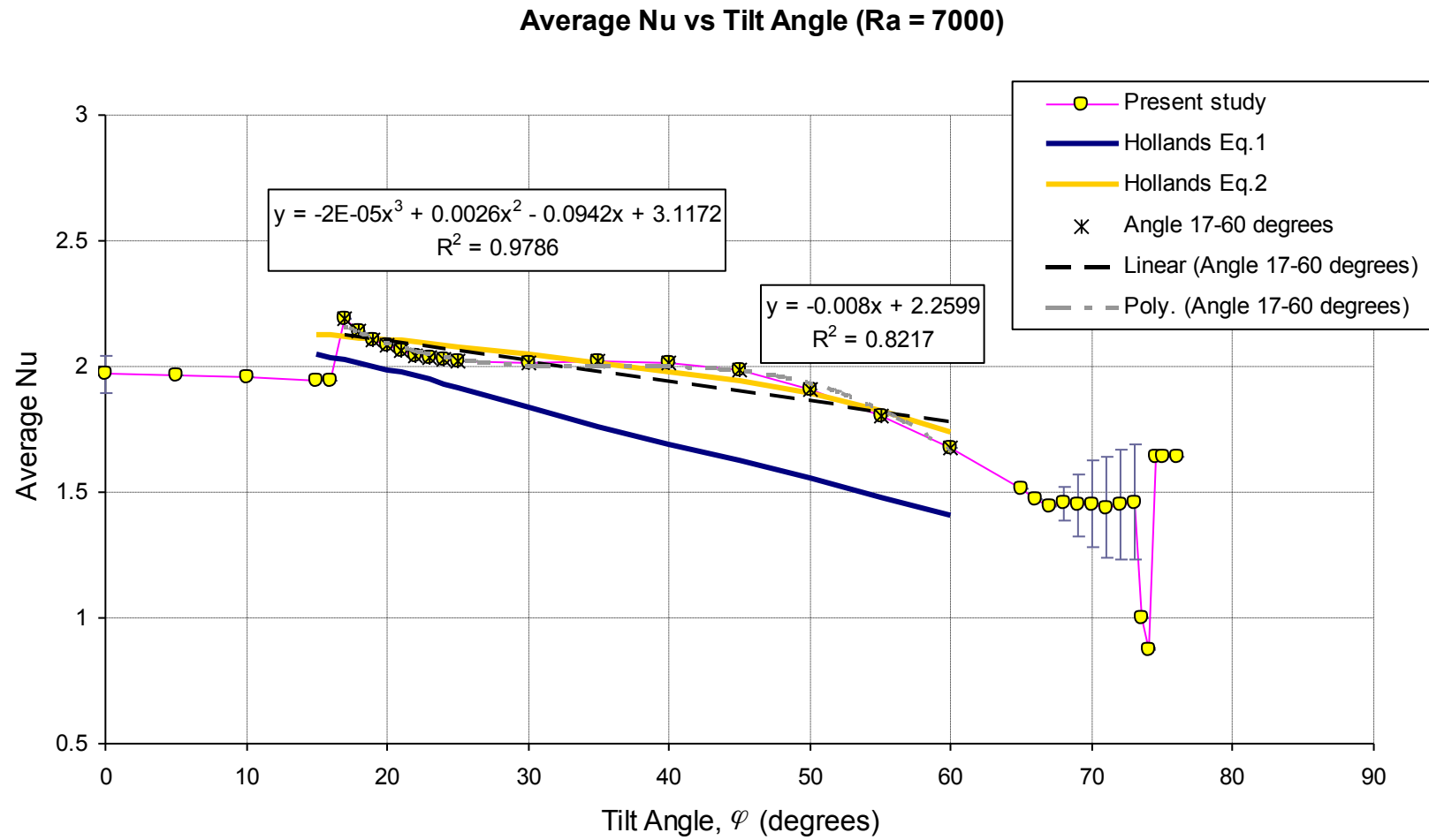


**Fig. 9**  $\overline{Nu}$  versus  $\varphi$ , for Ra = 7000

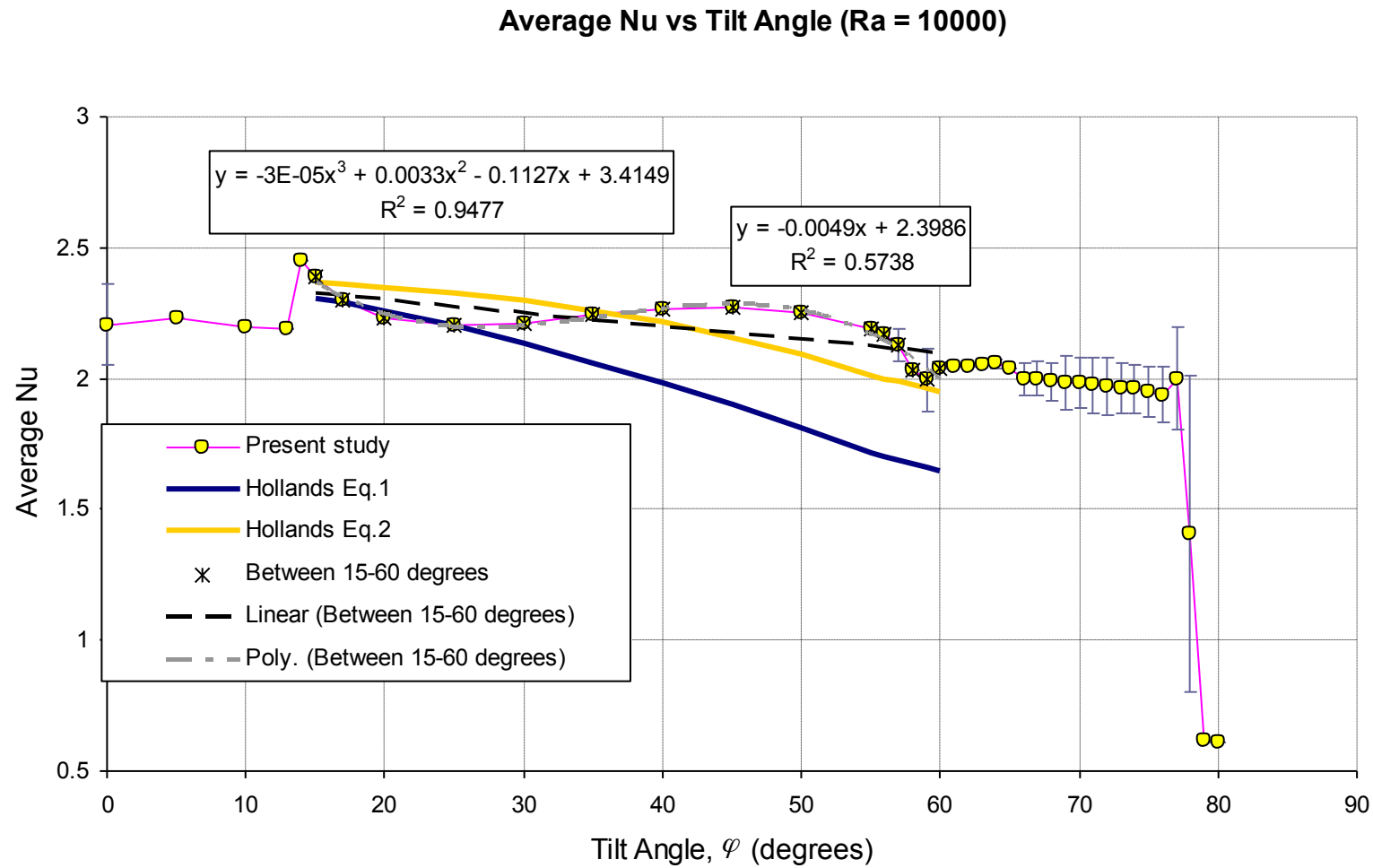
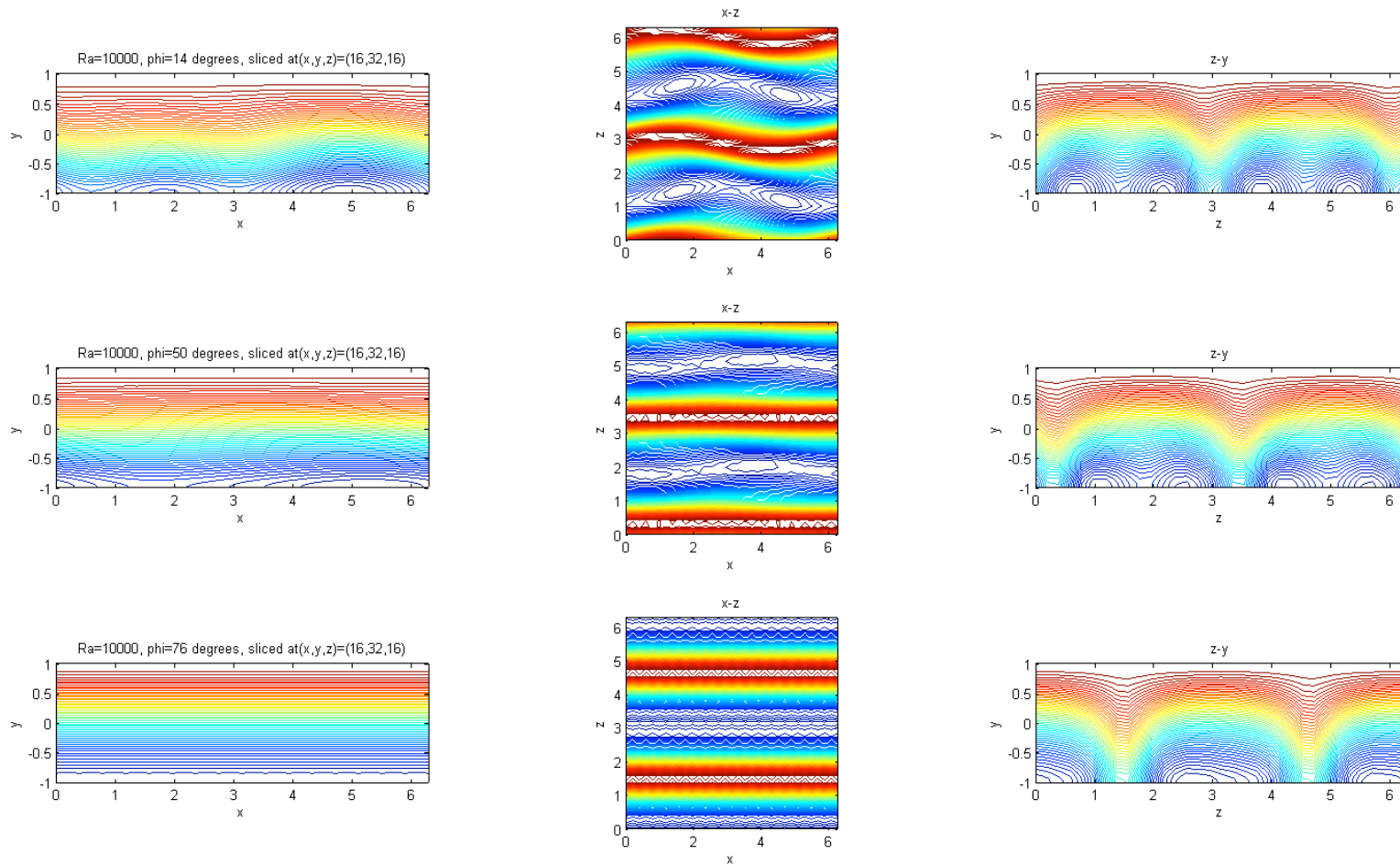


Fig. 10  $\overline{Nu}$  versus  $\varphi$ , for Ra = 10000

PREPRINT.

Ilker Tari, "Natural Convection Simulations and Numerical Determination of Critical Tilt Angles for a Parallel Plate Channel," Energy Conversion and Management, Vol. 51, No. 4, pp. 685-695 (2010).



**Fig. 11** Velocity fields for  $Ra = 10000$ ,  $\phi = 14^\circ$ ,  $50^\circ$ , and  $76^\circ$  at  $t^* = 30$ , sliced at the center planes

Average Nu vs  $Ra \cos \varphi$  (Ra=7000 and Ra=10000 data combined)

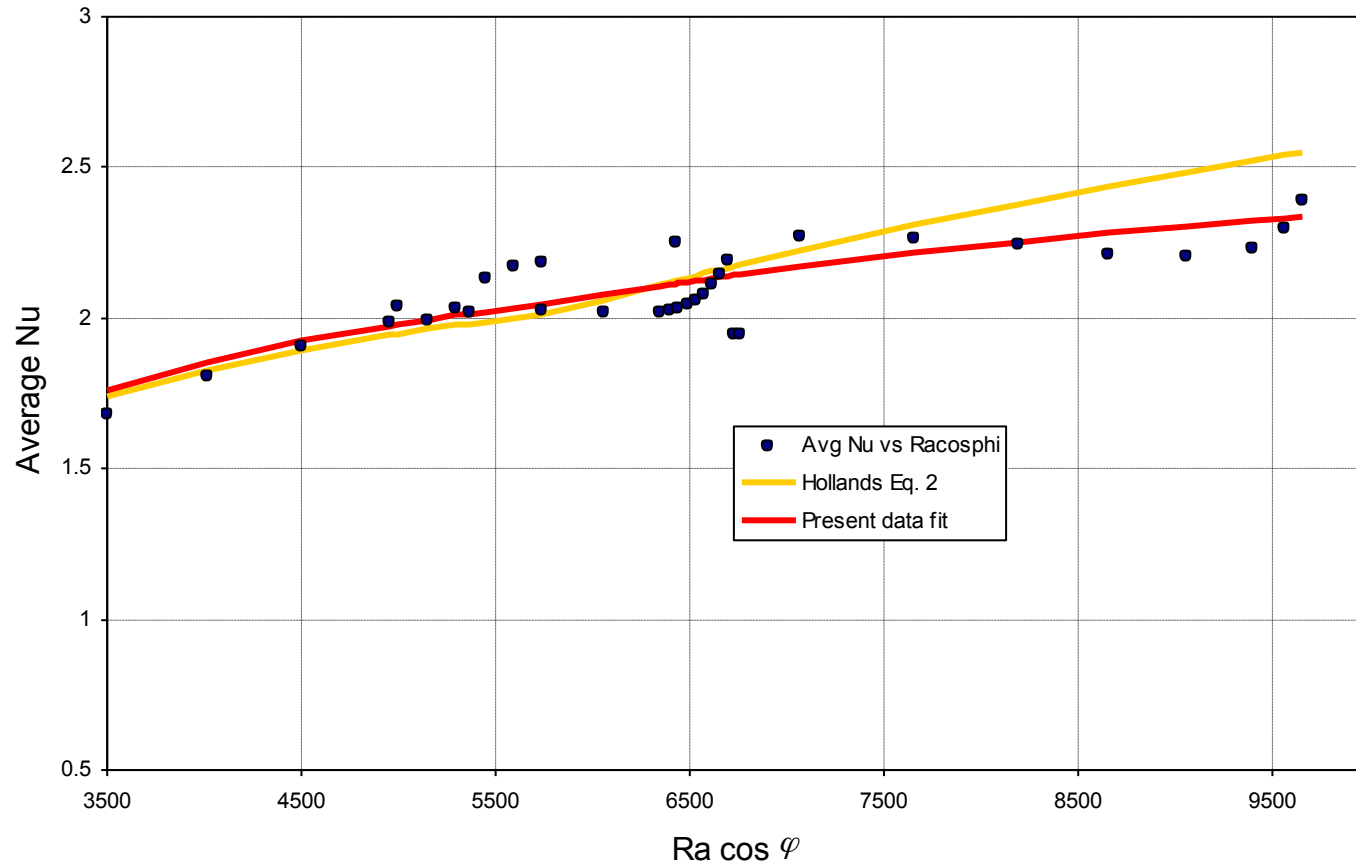


Fig. 12  $\overline{Nu}$  versus  $Ra \cdot \cos \varphi$ , for combined  $Ra = 7000$  and  $10000$  data